THE JOURNAL OF PHYSICAL CHEMISTRY B

ARTICLE

pubs.acs.org/JPCB

# Optical Properties of a Visible Push−Pull Chromophore Covalently Bound to Carbohydrates: Solution and Gas-Phase Spectroscopy Combined to Theoretical Investigations

Quentin Enjalbert,[†,¶,‡,§] Amandine Racaud,[†,¶,‡,§] Jérôme Lemoine,[†,¶,§] Sébastien Redon,[†,¶,∥,⊥] Mehmet Menaf Ayhan,[†,#] Chantal Andraud,[†,#] Stéphane Chambert,[†,¶,∥,⊥] Yann Bretonnière,[†,#] Claire Loison,[*,†,¶,‡] Rodolphe Antoine,[†,¶,‡] and Philippe Dugourd[†,¶,‡]

[†]Université de Lyon, F-69622, Lyon, France

[¶]Université Lyon 1, 43, Bld du 11 Novembre 1918, F-69622 Villeurbanne, France

[‡]Laboratoire de Spectrométrie Ionique et Moléculaire, UMR5579, CNRS, Université Lyon 1, France

[§]Laboratoire de Sciences Analytiques, UMR5180, CNRS, Université Lyon 1, France

[∥]Laboratoire de Chimie Organique et Bioorganique, INSA de Lyon, Lyon, France

[⊥]Institut de Chimie et de Biochimie Moléculaires et Supramoléculaires, UMR5246, CNRS, Université Lyon 1, INSA de Lyon, CPE-Lyon, Lyon, France

[#]Laboratoire de Chimie de l'ENS Lyon, UMR5182, CNRS, ENS Lyon, 46 allée d'Italie, F-69364 Lyon, France

Supporting Information

**ABSTRACT:** The use of visible absorbing and fluorescent tags for sensing and structural analysis of carbohydrates is a promising route in a variety of medical, diagnostic, and therapeutic contexts. Here we report an easy method for covalent attachment of nonfluorescent push−pull chromophores based on the 4-cyano-5-dicyanomethylene-2-oxo-3-pyrroline ring to carbohydrate moieties. The impact of sugar grafting on the optical properties of the push−pull chromophore in the gas phase and in solution was investigated by absorption and action spectroscopy and theoretical methods. The labeled sugars efficiently absorb photons in the visible range, as demonstrated by their intense photodissociation in a quadrupole ion trap. A strong blue shift (−70 nm) of the gas-phase photodissociation intensity maximum is observed upon sugar grafting, whereas no such effect is visible on the solution absorption spectra. Molecular dynamics simulations of labeled maltose in the gas phase describe strong interactions between the sulfonated chromophore and the carbohydrate, which lead to cyclic conformations. These are not observed in the simulations with explicit solvation. Time-dependent density functional theory (TD-DFT) calculations on model molecules permit us to attribute the observed shift to the formation of such cyclic conformations and to the displacement of the negative charge relative to the aromatic moiety of the chromophore.

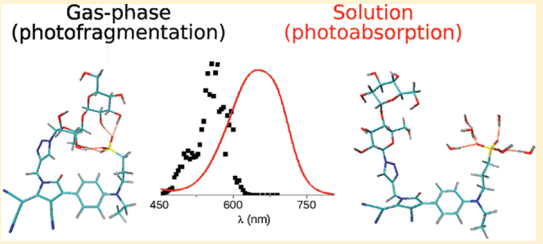


## INTRODUCTION

Sensing and structural analysis of carbohydrates is essential in a variety of medical, diagnostic, and therapeutic contexts.[1] Sensors based on amperometric measurements[2,3] using oxidative enzymes (oxidase or dehydrogenase)[4] for the detection of monosaccharides, or multienzyme biosensors for polysaccharides,[5] have been largely developed. Alternative approaches use optical spectroscopy, mostly through fluorescent labeling.[6,7] Fluorescent labeling of oligosaccharides is also frequently employed for the improvement of separation in high-performance liquid chromatographic and fluorophore-assisted capillary electrophoresis (FACE) analysis.[8,9] Most of the fluorescence detection methods are based on precolumn derivatization of carbohydrates by reductive amination via Schiff base in the presence of tag excess.[10] Nevertheless, it is often difficult to predict fluorescence intensities quantitatively, since depending on substituents, fluorescence enhancement or quenching can be observed. These labeling strategies are also a natural approach for implementation of ultraviolet photodissociation (UVPD) mass spectrometry (MS) for structural characterization of oligosaccharides, as illustrated in the pioneering works of Brodbelt and co-workers:[11,12] chromophores enhancing UV absorptivity grafted on oligosaccharides may enhance or facilitate ion photoexcitation.

These systems have excitation wavelengths in the UV or near-UV range. However, longer wavelength excitable fluorophores are highly desirable in order to make them compatible with

**Received:** October 14, 2011
**Revised:** November 30, 2011
**Published:** December 02, 2011

solid-state light sources like LEDs or diode pumped lasers. Furthermore, for an efficient transfer of the absorbed energy and enhanced ion dissociation, chromophores with weak fluorescence properties are required. In this context, we developed a series of push−pull chromophores in which the 4-cyano-5-dicyanomethylene-2-oxo-3-pyrroline ring acts as an electron acceptor during photoabsorption (see Scheme 1).

These compounds were originally reported for their good light fastness properties in the early 1960s in a patent dealing with textile coloring[13] and since have been described in another textile patent.[14] Their ease of synthesis and their absorption wavelength in the visible made them very attractive. It is only very recently that the 4-cyano-5-dicyanomethylene-2-oxo-3-pyrroline ring was used as a functionalized powerful electron-accepting group for push−pull dipolar compounds having strong second-order nonlinear properties.[15] Alkylation or acylation are possible on the N-1 nitrogen atom of the oxo-pyrrolidine ring and permit the functionalization of the chromophore for various applications. It is worth mentioning that no fluorescence properties have been reported to date.

In this paper, we aim at exploring the optical properties of push−pull chromophores based on the 4-cyano-5-dicyanomethylene-2-oxo-3-pyrroline ring by spectroscopic and theoretical methods. The bare chromophore and its corresponding derivatives covalently bound to carbohydrates were investigated in solution and in the gas phase. Studies in solution permit us to address the influence of the solvent polarity on their absorption properties. On the other hand, gas-phase studies allow us to eliminate spurious intermolecular and/or solvent−molecule interactions. It allows us therefore to study the bare chromophore and its corresponding derivative covalently bound to carbohydrates in a well-defined initial state and to characterize intrinsic intramolecular interactions. The impact of sugar grafting on the optical properties of the chromophore in the gas phase is important and should be taken into account to exploit quantitatively the optical response of various labeled carbohydrates. To better address this issue, the bare chromophore and its derivatives were also studied theoretically. The impact of sugar grafting on the optical properties of the chromophore depends on (i) the sugar−chromophore interactions and (ii) on the variability of the chromophore optical properties. To investigate the first point, molecular dynamics simulations were performed. They have proved to be adapted to describe the molecular interactions within carbohydrates,[16,17] even if force fields are still under development.[18−27] The particularity of sugars relative to other biomacromolecules is their floppiness and the necessity to sample the phase space during long times. Various methods to enhance the conformational sampling may be applied, for example, replica exchange molecular dynamics,[28] which was also chosen here. To investigate the optical properties of the chromophore, time-dependent density functional theory (TD-DFT)[29−31] or multiconformational approaches (e.g., CASSCF[32−34]) offer nowadays a satisfactory compromise between accuracy of the predictions and calculation cost. However, the conformations of the tagged sugars obtained by molecular dynamics using force field approaches are not expected to be accurate enough for the prediction of the spectroscopic properties. Indeed, in the present case, the sugar acts as an electrostatic embedding to the chromophore and also imposes mechanical deformations on the chromophore. Both actions may modify significantly the electronic structure of the very polarizable chromophore, and consequently the force-field parameters. Mixed classical/quantum description (QM/MM)[35] could be a challenging approach for such systems, with a quantum description of the chromophore and a classical model for the sugar. However, the coupling of the QM and MM descriptions gives rise to efficiency and accuracy limitations when the QM wave function is strongly affected by an MM electrostatic potential, and when both the QM and the MM conformations are influenced by their

**Scheme 1. Push−Pull Molecules Are Composed of a $\pi$-Conjugated Bridge Connecting an Electron Donor Moiety to an Electron Acceptor Moiety[a]**

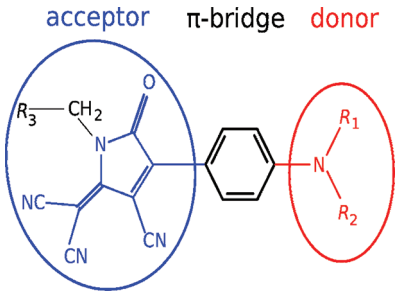


[a] In the present work, the 4-cyano-5-dicyanomethylene-2-oxo-3-pyrroline ring is the acceptor (left) and the dimethylamino group is the donor (right).

**Scheme 2. Synthesis of Chromophore 1[a]**

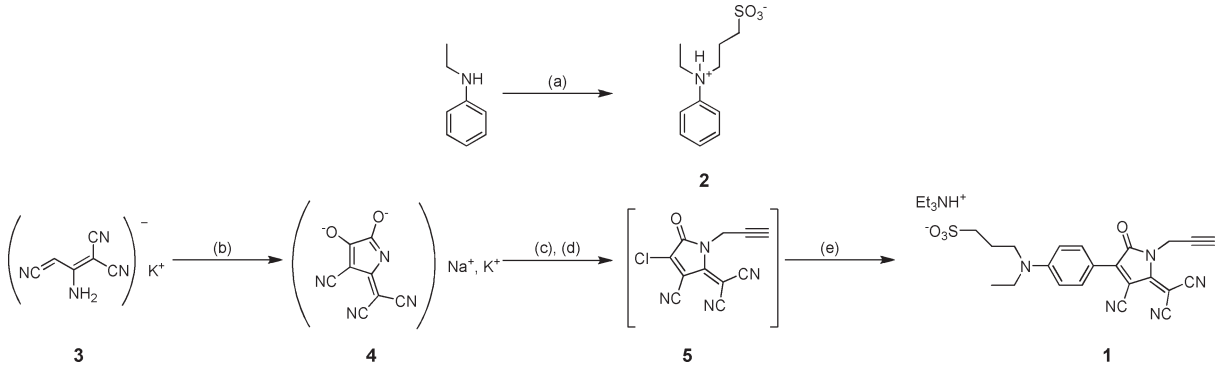


[a] Reagents and conditions: (a) propanesultone, 1,1,1-trichlorethane, reflux; (b) NaEtO, dry ethanol, then diethyl oxalate, 3 h, r.t., 95%; (c) propargyl bromide, dry DMF, 90 °C, 4 h; (d) $SOCl_2$, dry DMF, 0−5 °C, 3 h, 80%; (e) **2**, dry DMF, $Et_3N$, 0−5 °C, 3 h; 86% for the three steps.


dx.doi.org/10.1021/jp2099015 |J. Phys. Chem. B 2012, 116, 841–851

**Scheme 3. Synthesis of the Tagged Sugars 8 and 9**[a]

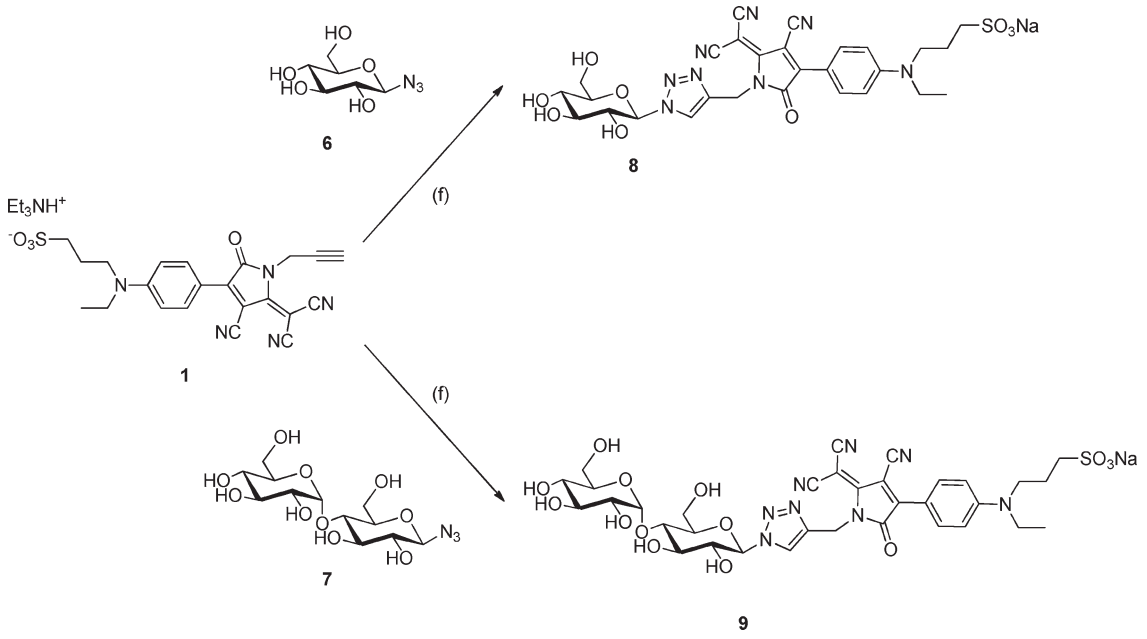


[a] Reagents and conditions: CuI (10%), MeOH, sealed tube, 110 °C, 2 h, microwave irradiations, 61−85%.

coupling.[36] In the present work, classical molecular dynamics simulations are used to provide a qualitative picture of the sugar conformations and are accompanied by separate quantum chemistry calculations of the optical properties of relevant model molecules.

## EXPERIMENTAL SECTION

**Chromophore Synthesis and Sugar Derivatization.** We chose here to develop a multistep one-pot procedure for the formation of an N-alkylated 4-cyano-5-dicyanomethylene-2-oxo-3-pyrroline-based chromophore. The functional group introduced is a terminal alkyne that will be further used in copper(I) alkyne−azide cycloaddition with an azido-functionalized biomolecule for the coupling strategy. The chromophore **1** bearing a terminal alkyne group was obtained in a five-step sequence (Scheme 2) in which three steps were run in a one-pot procedure.

The sulfonic acid salt **1** was obtained by alkylation of *N*-ethylaniline with propanesulfone in refluxing 1,1,1-trichloroethane. The potassium salt of malononitrile dimer **3** (obtained in very good yield from malonitrile and potassium hydroxide in ethanol as described by Mittelbach[37] was converted to the mixed salt of 4-cyano-5-dicyanomethylene-3-hydoxy-2-oxo-3-pyrroline (**4**) by reaction with diethyl oxalate and sodium ethoxide in ethanol.[14] The next three steps were run successively without intermediate purification. First, **4** was selectively N-alkylated with propargyl bromide in DMF at 90 °C and further transformed to the highly unstable chloro compound **5** by reaction with thionyl chloride in DMF at 0 °C. Then, reaction of **5** with *N*-ethyl-*N*-propanesulfonylaniline immediately gave the desired compound **1** in moderate yield. The coupling procedure of the chromophore **1** with 6-azido-6-deoxy-sucrose (**6**) involved the use of Cu(I) as a catalyst in a MeOH/$CH_3Cl$ mixture at 50 °C (Scheme 3).

The chromophore **1** was introduced on pure anomeric form of monosaccharide **6** and disaccharide **7**. To this end, the carbohydrate azides **6** and **7** were obtained stereoselectively with a $\beta$ configuration by reacting DMC (2-chloro-1,3-dimethylimidazolinium chloride) and sodium azide with the corresponding unprotected mono- or disaccharide in aqueous media.[38] Several reactive conditions were tested, including the standard CuI classical procedure using different solvent systems ($CH_2Cl_2$/MeOH, $CHCl_3$/MeOH) and different temperatures (50−66 °C). Even after prolonged reaction time (up to 24 h) the obtained yields were unsatisfactory (below 35%). Thus, coupling was optimized under microwave irradiations[39] in the appropriate sealed tubes using CuI as a catalyst in MeOH at 110 °C (Scheme 3). The final compounds were purified as detailed in the Supporting Information.

**UV−Vis Absorption in Solution.** UV−vis absorption spectra were recorded on a JASCO V550 spectrometer. All solvents were of spectrophotometric grade.

**Mass Spectrometry and Visible Photodissociation.** The experimental setup consists of a mass spectrometer coupled to a visible/UV tunable OPO laser. The mass spectrometer is a quadrupole linear ion trap (LTQ; Thermo Fisher Scientific, San Jose, CA, U.S.A.).[40,41] A quartz window was fitted on the rear of the LTQ chamber to allow the introduction of the laser beam. The OPO laser (Panther OPO laser pumped by a 355 nm Nd:YAG Surelite; Continuum, Santa Clara, CA, U.S.A.) can be scanned from 215 nm up to 2 $\mu$m. Its main characteristics are a repetition rate of 10 Hz and a pulse width of 7 ns. The laser beam passes through two diaphragms, lenses (3:1 telescope), and a mechanical shutter electronically synchronized with the mass spectrometer, after which it is injected on the axis of the linear trap through a 1 mm diameter pinhole. The laser energy after the pinhole is between 0.1 and 1 mJ/pulse. The mechanical shutter is used to synchronize laser irradiation with ion trapping. To perform laser irradiation for a given number of laser pulses, we add an $MS^n$ step with activation amplitude of 0% in the ion trap rf sequence, during which the shutter located on the laser beam is


dx.doi.org/10.1021/jp2099015 |*J. Phys. Chem. B* 2012, 116, 841–851

**Scheme 4. Model Molecule Studied Theoretically and Various Notations for Atoms, Structural Parameters, and Interactions Relevant for the Discussion**[a]

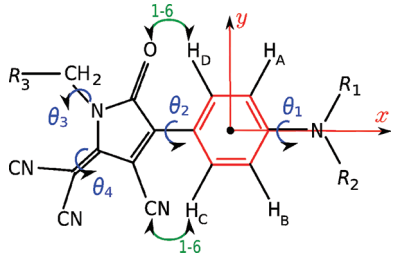


[a] The substituent $R_1$ is a methyl or ethylsulfonate, $R_2$ is a methyl or an ethyl, and $R_3$ is a methyl, ethyne, or the triazole branched maltose (as in compound **9**). The axes are defined relative to the phenyl ring as depicted on this scheme; the origin is at its center, and the *z*-axis is perpendicular to its plane.

opened. The laser power is monitored in front of the mass spectrometer by a power meter (Ophir, Logan, UT, U.S.A.).

In the UVPD experiments, precursor ions were first isolated in the trap. After isolation, they were irradiated for *n* laser shots, and the resulting mass spectrum was recorded. Optical spectra (action spectra) were obtained by systematically recording UVPD spectra as a function of the laser wavelength. The yield of fragmentation ($\sigma$) was plotted as a function of the laser wavelength, as defined by $\sigma = \ln((\text{precursor} + \Sigma\text{frag})/\text{precursor})/\phi)$, where $\phi$ is the laser fluence, precursor is the intensity of the precursor peak, and Σfrag represents the total intensity of the photofragment peaks. Collision-induced dissociation (CID) experiments were performed with the same apparatus. This was accomplished using helium gas at a normalized collision energy of 13−15% for 30 ms. The activation *q* value was set to 0.200 for CID and for UVPD. The isolation width for selecting the ion precursors (both for UVPD and CID) was 3 Da. A total of 50 microscans were averaged to produce a spectrum.

## THEORETICAL INVESTIGATION

**Electronic Structure Calculations on Model Chromophores.** Model chromophores (see Scheme 4) have been studied in order to estimate the impact of structural parameters on the optical response of 4-cyano-5-dicyanomethylene-2-oxo-3-pyrroline. The substituent $R_1$ is a methyl or ethylsulfonate, $R_2$ is a methyl or an ethyl, and $R_3$ is a methyl, ethyne, or the triazole branched maltose (as in compound **9**).

Calculations have been performed with the ADF[42] and Gaussian[43] suites of programs. The ground-state geometries have been obtained using DFT optimization (residual gradient $<10^{-5}$ au) using the frequently used BP86 functional[44,45] and the M062X functional developed by Zhao and Truhlar to describe accurately weak intermolecular interactions.[46] The basis set was composed of triple-ζ orbitals augmented by polarization and diffusion functions (ATZ2P for Slater-type or 6311+G* for Gaussian-type). The excitation energies have been determined with TD-DFT as implemented in the Amsterdam Density Functional program (ADF2010).[47] The exchange and correlation kernel is the adiabatic linear density approximation (ALDA)[48] with the statistical average of orbital potential (SAOP) functional.[49] The latter has correct asymptotic behavior proportional to $1/r$ when $r$ tends to infinity ($r$ is the distance between two charges). Bulk solvent effects have been included using the polarizable continuum model (PCM),[50] which is able to obtain a valid approximation for solvent effects as long as no specific interactions link the solute to the solvent molecules. The variation of the excitation energies upon deformations along each single vibrational mode was calculated using a locally modified version of the program Gabedit,[51] adapted to generate conformations with phonon amplitude corresponding to a fixed energy (10 kJ·mol$^{-1}$). The excited-state dipole moment of the chromophore was calculated at the B3LYP/6-311+G*//SAOP/ATZ2P level by a derivative calculated with a five-point stencil using static electric fields (0, ± 0.005 au, and ±0.010 au).

**Force Field Modeling of Chromophore-Derivated Maltose.** The parameters for the maltose were the ones developed by Damm et al.,[18] and the ones for the triazole ring were chosen by analogy with the parameters of relevant N-containing heterocycles.[52] The parameters describing the chromophore were chosen by analogy with similar biomolecules or extracted from quantum chemistry calculations. Atom-centered point charges of the chromophore atoms have been derived from the restrained electrostatic potential (RESP)[53] on fragment molecules at the HF/6-31G//HF/6-31G level[54,55] and were found to be close to the one obtained using the automatic parametrization developed by Jorgensen and Tirado-Rives.[56] The negative charge of the sulfonated chromophore is located on the sulfonate group. Taking compound **1** as reference, the Ryckaert Bellemans parameters linked to three dihedral angles describing low-energy deformations ($\theta_1$, $\theta_2$, and $\theta_4$ of Scheme 4) have been optimized to map the MM potential energy onto M062X/6-311+G* total energy curves. The optimization tool was based on the Automated Frequency Matching Method program (AFMM),[57] which has been locally modified to use the Nelder−Meade amoeba method[58] and to use the GROMACS package for MM calculations. The minimized function was a linear combination of the mean-square deviation between the two energy curves and the root-mean-square displacement between the optimal geometries of the QM and MM models (final value of 0.1 Å). The comparison of the quantum and classical energies for the dihedral angle $\theta_2$ between the two aromatic rings of compound **1** (see Scheme 4) is given in the Supporting Information (see Figure S8). Noticeably, for this specific angle, the 1−6 Coulomb and Lennard-Jones interactions highlighted in Scheme 4 had to be optimized in parallel to the Ryckaert Bellemans dihedral parameters to get a correct description of the small energy barrier encountered when the two aromatic cycles become coplanar. Comparison of energy curves for the dihedral angles $\theta_1$, $\theta_3$, and $\theta_4$ are reported as Supporting Information (Figures S7, S9, and S10). In summary, the OPLS-AA model has been mainly constructed using existing parameters, but special care has been taken for the parametrization of the dihedral angles describing the soft deformations of the chromophore.

**Replica-Exchange Molecular Dynamics Simulations.** The conformational landscape of the generated model in the gas phase has been explored using replica-exchange molecular dynamics (REMD) simulations[59,60] as implemented in GROMACS-4.5.4.[61] Integration of equations of motion have been performed using a velocity verlet algorithm, with constraints on hydrogen-carrying bonds, a dielectric constant of 1, a cutoff for the electrostatic forces at 15 nm with a switch at 10 nm. The duration of the trajectories was 50 ns at each temperature. Canonical thermalization was achieved using a velocity-rescaling thermostat[62] with a coupling of 5.0 ps for 28 trajectories carried out between 65 and 2800 K. A time-step as small as 0.5 fs was necessary to enforce the numerical conservation of the velocity-rescaling

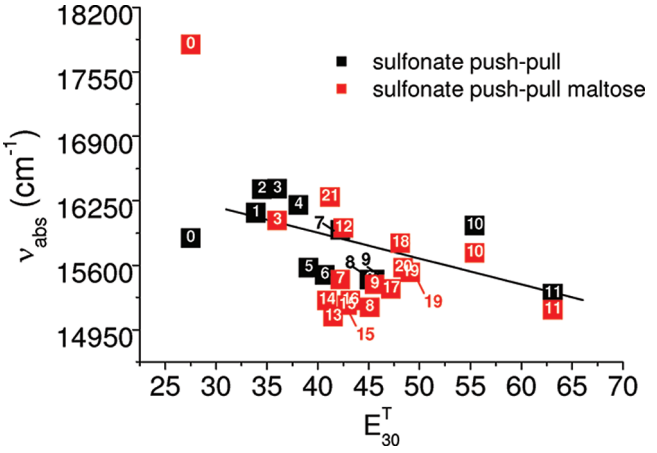


**Figure 1.** Plots of absorption maxima in various solvents vs the solvent polarity $E_{30}^T$ for the bare push−pull sulfonate chromophore (compound **1**, black squares) and covalently bound to maltose (compound **9**, red squares). The black line corresponds to the linear fit of the absorption maxima vs $E_{30}^T$ for the bare push−pull sulfonate chromophore (black squares). (1, toluene; 2, ether; 3, dioxane; 4, EtOAc; 5, chloroform; 6, dichloromethane; 7, acetone; 8, DMSO; 9, MeCN; 10, MeOH; 11, water; 12, butyronitrile; 13, benzonitrile; 14, HMPA; 15, DMAc; 16, DMF; 17, cyclohexanol; 18, octanol; 19, pentanol; 20, isopropyl alcohol; 21, nitrobenzene; 0 represents the gas-phase data).

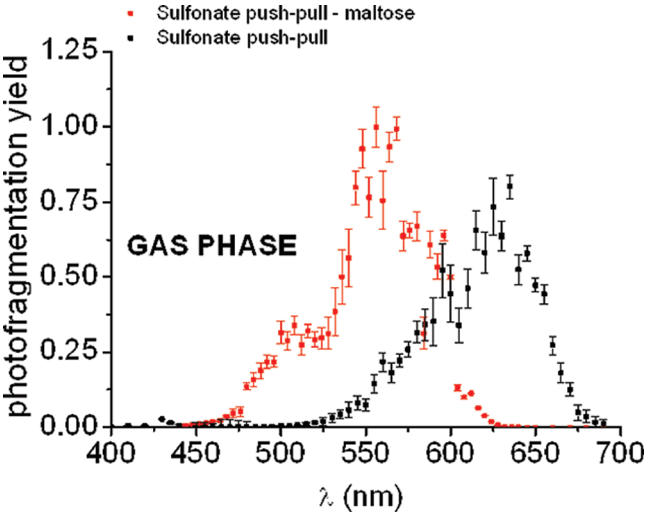


**Figure 2.** Experimental gas-phase photofragmentation yield of push−pull sulfonate chromophore isolated (compound **1**, black squares) and covalently bound to maltose (compound **9**, red squares). The definition of the yield is given in the Experimental Section.

conserved energy, i.e., a correct description of energy fluctuations of the canonical ensemble and a minimal distortion of the conformational space due to the replica exchange.[63] The choice of such a high maximal temperature was guided by the necessity to break noncovalent bonds between the sulfonated anion and the maltose hydroxyls. Initial conformations have been thermalized during 50 ps before beginning the temperature exchange. A first REMD of 10 ns is done to get 10−20 various low-energy structures, and then a second 50 ns REMD is launched with these structures as initial points. The exchange between pairsof configurations from adjacent replicas was attempted every 100 fs,[64] and the configurations were recorded every 200 ps. The temperature exchange probability upon the whole temperature range averages between 0.2 and 0.5. Analysis and visualization were done using the Visual Molecular Dynamics (VMD) program.[65]

The conformational landscape of the generated model in water has been explored using molecular dynamics simulations in explicit solvent (TIP3P)[66] at 300 K. The simulations are carried out without replica exchange during 50 ns and using a specific potential for the dihedral angle $\theta_2$ (see the Supporting Information).

## RESULTS AND DISCUSSION

In the following, the experimental optical properties of the bare chromophores and the grafted carbohydrates in solution and in the gas phase are discussed first. The chromophore−sugar interactions predicted by molecular dynamics simulations and the impact of various structural parameters on the optical properties of the chromophore presented in a second part permit us to further discuss the experimental data.

**A. Absorption Spectra in Solution.** The visible absorption spectra of the bare push−pull sulfonate chromophore **1** and the one covalently bound to maltose **9** have been investigated in various solvents of different polarities and hydrogen-bond donating abilities. The absorption spectra of the bare push−pull sulfonate chromophore display an intense broad band in the 500−750 nm range (see the Supporting Information). The band position depends on the solvent, whereas its shape is independent of the solvent used. With increasing the solvent polarity from toluene to water, the visible absorption spectra of the bare push−pull sulfonate show a red shift of the visible band. The correlation between the absorption spectra and dielectric solvent properties can be figured out by plotting the absorption maxima versus the solvent polarity using the Reichardt scale ($E_{30}^T$)[67] (see Figure 1). This solvatochromism may be attributed to a better stabilization of the molecule in the first excited state relative to that in the ground state, with increasing solvent polarity. This suggests that the dipole moment is larger in the excited state than in the ground state, in accordance with our theoretical results (see below).

The absorption spectrum of the push−pull chromophore covalently bound to maltose displays a more complex dependence with respect to the solvent as compared to the bare chromophore. For the less polar solvents (chloroform, dichloromethane, ether, ethyl acetate, and toluene), a double-band pattern is observed. Concentration dependence absorption experiments indicate that the push−pull chromophore covalently bound to maltose is subject to aggregation; therefore, the absorption spectra were not exploited further. For polar solvents (acetone, acetonitrile, dimethyl sulfoxide, methanol, and water), absorption bands are very similar to the ones recorded for the bare compound (see the Supporting Information). For solvents with intermediate polarity (acetone, alcohols, and acetonitrile), the absorption bands are slightly red-shifted. For the maltose-grafted chromophore, as for the bare chromophore, the absorption maxima are slightly red-shifted when the solvent polarity increases. In summary, the sugar has a weak influence on the optical properties of the push−pull chromophore in solution.

**B. Visible Photodissociation and Gas-Phase Action Spectra.** Besides fundamental aspects of the solvation properties of push−pull molecules, an important finding is that derivatized sugars display a strong absorption in the visible range. Whereas high photon energy is usually required for the photofragmentation of native oligosaccharides,[41,68−72] derivatization with such push−pull chromophores allows us to use visible light for inducing photofragmentation of carbohydrates. To delineate


dx.doi.org/10.1021/jp2099015 |J. Phys. Chem. B 2012, 116, 841–851

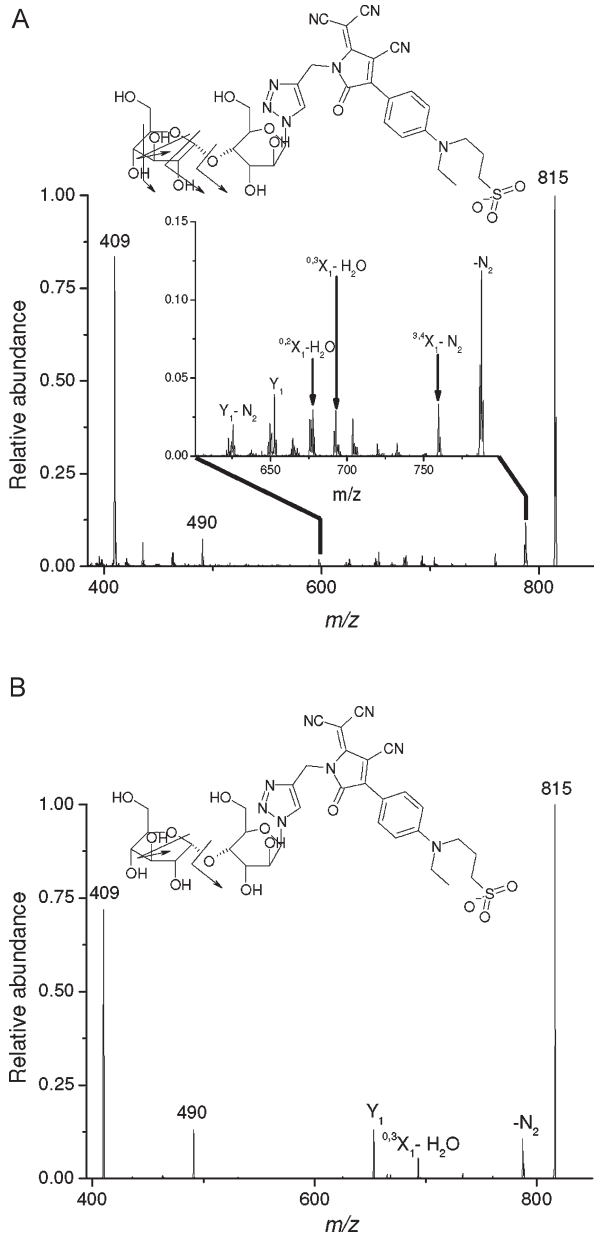


**Figure 3.** (A) Photofragmentation and (B) CID mass spectra recorded for isolated push−pull sulfonate chromophore covalently bound to maltose (compound **9**). Photofragmentation experiments were done at $\lambda$ = 560 nm (five laser shots). Main observed cleavages are shown on the schematic structures.

the wavelength ranges that could be used in the visible range to fragment chromophore-labeled carbohydrates, we recorded the gas-phase optical spectra as a function of laser wavelength for the push−pull chromophore covalently bound to maltose. Note that these spectra can serve as benchmarks for addressing environmental effects (in particular solvation) on such systems.

The sulfonate moieties of the push−pull chromophores (bare or covalently bound to maltose) are completely deprotonated in water. In the MS spectrum of such molecules, the molecular ions correspond to anionic species with a single charge located on the sulfonate group ($SO_3^-$). All experiments for optical properties study, as well as comparisons of the UVPD and CID dissociation pathways, were performed on the such singly charged species.

The measurement of the fragmentation yield for the sulfonate push−pull chromophores covalently bound to maltose, which reflects the action spectrum, displays a broad band with a maximum at $\lambda \sim 561$ nm (17 825 $cm^{-1}$) and an additional shoulder at $\lambda \sim 500$ nm (20 000 $cm^{-1}$), which may emerge from the vibrational structure of the same electronic excitation (see Figure 2). In order to better address the effect of the carbohydrate molecule on optical properties of push−pull chromophore, we recorded fragmentation yield for the bare sulfonate push−pull chromophore. The action spectrum for the bare chromophore displays a broad band with a maximum at $\lambda \sim$ 630 nm (15 873 $cm^{-1}$) and an additional shoulder at $\lambda \sim 580$ nm (17 241 $cm^{-1}$) (see Figure 2). The presence of the maltose covalently bound to the push−pull chromophore considerably affects the action spectra via a strong blue shift (of ∼70 nm). This shift, much larger than what is expected from a linear interpolation of solution data (see Figure 1), is discussed in details in section C.

Another interesting point concerns the fragmentation products observed after visible irradiation of sulfonate push−pull chromophores covalently bound to maltose. Figure 3A displays the photofragmentation mass spectrum recorded after irradiation of ions with five laser pulses at $\lambda$ = 560 nm. Figure 3B provides the corresponding CID spectrum. In the case of a single-shot irradiation (data not shown), identical photofragments with similar relative abundances were observed but of lower signal intensities. Intense fragments ($m/z$ 409 and 490) correspond to the cleavages before and after the triazole ring. Most of the fragment ions produced by CID are also observed in visible photodissociation mode. This is an indication that most of the UVPD fragmentation occurs after energy redistribution to vibrational modes (also called internal vibrational energy redistribution, or IVR) of the precursor ions. Some fragments are observed between $m/z$ 600 and $m/z$ 800 and arise from the fragmentation of the sugar bonds with the preservation of the intact chromophore. Note that a $Y_1$ fragment is also observed both in CID and visible photodissociation. Additional fragments, only observed in the visible photodissociation mode, are attributed to cross-ring cleavages (X-like ions). Interestingly, while the initial excitation is located on the push−pull molecule, numerous fragments are observed in the sugar moieties, meaning that efficient energy redistribution occurs in such tagged carbohydrates. Similar results are observed with push−pull molecules bound to monosaccharide (see Figure S5 of the Supporting Information).

**C. Theoretical Investigation of Structural and Optical Properties of Push−Pull Chromophore and Derivatives Covalently Bound to Carbohydrates.** The molecular dynamics simulations of the chromophore and its modification upon sugars grafting are discussed first. For comparison, both neutral and anionic sulfonated chromophores have been investigated (in Scheme 4, the substituent $R_1$ is either a methyl or an ethylsulfonate). Then, TD-DFT calculations of the optical excitations are exploited to interpret the experimental absorption and photofragmentation spectra.

*C.1. Conformations of the Bare and Sugar-Grafted Chromophore.* The N-alkylated 4-cyano-5-dicyanomethylene-2-oxo-3-pyrroline forms a conjugated ring and is therefore planar. The coplanarity of the aniline and the pyrroline is favored by an aromatic delocalization of the $\pi$ electrons on both rings, but steric repulsions between the substituents impede a perfect coplanarity. According to the DFT geometry optimizations, in vacuum the optimum dihedral angle between the two rings ($\theta_2$ in

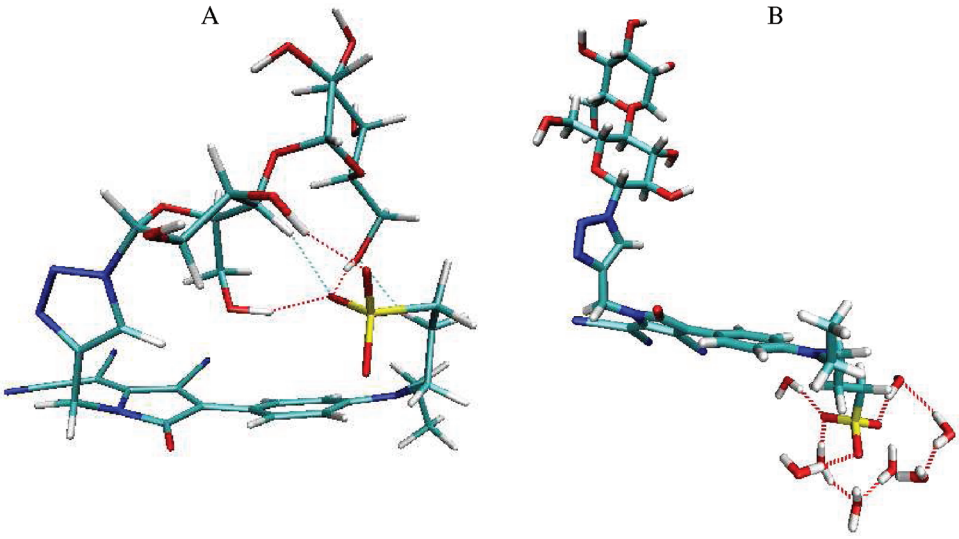


**Figure 4.** Typical low-energy conformations of compound **9**: (A) in vacuum; (B) in water (explicit solvation, water molecules not shown except those in the vicinity of the sulfonate group). Color code: blue = nitrogen, cyan = carbon, red = oxygen, yellow = sulfur, white = hydrogen.

Scheme 4) lies around 20°. The $^1$H NMR spectrum of the neutral compound **1**, which shows a single resonance for hydrogens A and B, and also for hydrogens C and D (see Scheme 4), indicates rotations of the substituents of the aromatic rings at room temperature (see the Supporting Information). In addition to this flexibility of the aromatic cycles, the sulfonated molecules show many conformations of similar energies because of the flexible tail bearing the sulfonate group. Typically for gas-phase calculations of the sulfonated chromophore (molecule **1**), after PM6 optimization of the REMD conformations at 320 K, 44 different conformations were obtained within an energy range of $3k_BT$ above the energy minimum.

When the sugar is added, two contradictory effects influence the conformational landscape: on one hand, the sugar moieties bring a large flexibility, but on the other hand, strong end-to-end sugar−sulfonate interactions constrain the molecule. At ambient temperature, and in vacuum, all the conformations obtained by the simulations form a closed ring (see Figure 4A). Figure 5A depicts the probability distributions of the sulfur position along the $x$-axis and of the dihedral angle $\theta_2$ obtained by the REMD at 320 K for the bare chromophore (molecule **1**) and the maltose-grafted chromophore (molecule **9**). The main result is that the maltose presence shifts the sulfonated group closer to the benzene ring (centered at $x = 0$); a small increase of $\langle\theta_2\rangle$ is also observed. For the bare chromophore (solid lines), the distribution of the sulfur position is binodal and appears in fact relatively sensitive to the MD parametrization. According to DFT calculations at the M062X/6311+G* level, the peak at $x = 7.5$ Å indeed corresponds to lower total energies. When the maltose is present, the sulfur position is restrained to a single peak with an average value of $\langle x\rangle = 2.2 \pm 0.1$ Å corresponding to cyclic conformations as the one shown in Figure 4A. Interestingly, the chromophore−hydroxyl proximity may favor an energy transfer from the chromophore to the maltose, which could lead to the fragmentation patterns observed experimentally (see Figure 3).

The effect of water solvation on the grafted maltose is illustrated in Figures 4B and 5B. The intermolecular solvation of the sulfonated tail favors open conformations (see Figure 4B). The corresponding probability distributions of $x$ and $\theta_2$ (Figure 5B) show that the dihedral angle of the solvated chromophore fluctuates more with a higher average value. No cyclic conformations are observed in solution (during the limited sampling of the simulation).

To conclude, in vacuum, the sugar grafting imposes a mechanical constraint on the chromophore, which influences strongly its conformational landscape and favors cyclic conformations. In water, the maltose grafting has no such effect on the chromophore. The coupling between the elastic and optical properties of the chromophore may be the origin of the shift upon sugar grafting in the photodissociation spectra observed experimentally (see Figure 2) and of the difference observed between gas phase and solution spectra (see Figure S4a in the Supporting Information).

*C.2. Optical Properties of Neutral and Anionic Model Chromophores.* To understand how such sugar−chromophore interactions influence the experimental action spectra, the vertical electronic excitations of model chromophores (Scheme 4) have been investigated using quantum chemistry calculations (TD-DFT).

*C.2.1. Photoexcitation of the Neutral Nonsulfonated Chromophore.* For push−pull aromatic chromophores, the absorption in the UV−vis range corresponds to electronic excitations from the highest occupied molecular orbital (HOMO) $\pi$ orbital to the lowest unoccupied molecular orbital (LUMO) $\pi^*$ orbital. For the neutral chromophore (Scheme 4 with $R_1$ = Me, $R_2$ = Me, $R_3$ = CCH), the HOMO and LUMO are localized solely on the aromatic rings (see Figure 6A). The HOMO shows a larger contribution on the dimethylaminophenyl, which plays the role of donor in the intermolecular charge transfer upon electronic excitation, whereas the LUMO plays the role of acceptor and is located on the pyrroline ring. Such an intermolecular charge transfer upon excitation is characteristic of push−pull chromophores. Our TD-DFT calculations predict a dipole moment along the molecular axis increasing from 12.7 to 16.8 D upon excitation, which sustains our interpretation of the solvatochromism observed experimentally (see Figure 1): a more polar solvent stabilizes more the excited state than the ground state. This effect can also be reproduced by a polarizable continuum solvation model (PCM): for a fixed geometry (optimized at the


dx.doi.org/10.1021/jp2099015 |J. Phys. Chem. B 2012, 116, 841–851

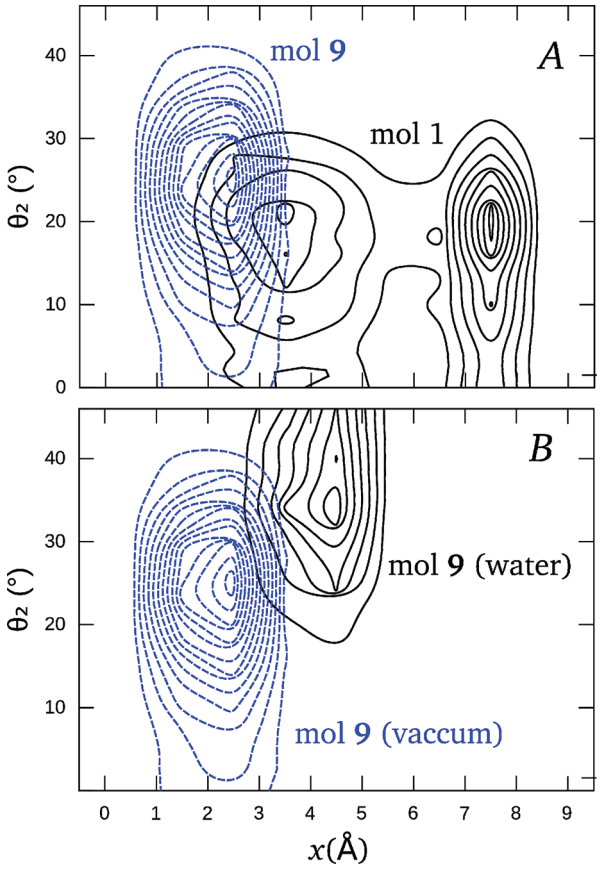


**Figure 5.** Isocontours (arbitrary units) of the probability distribution of the dihedral angle $\theta_2$ and of the position of the sulfonate group along the $x$-axis obtained by the MD calculations (see Scheme 4). (A) Comparison between the bare chromophore (compound **1**, solid lines) and the maltose-grafted chromophore (compound **9**, dashed lines) in the gas phase at 285 K. (B) Comparison between compound **9** in the gas phase at 295 K (dashed lines) and in water at 300 K (solid lines).

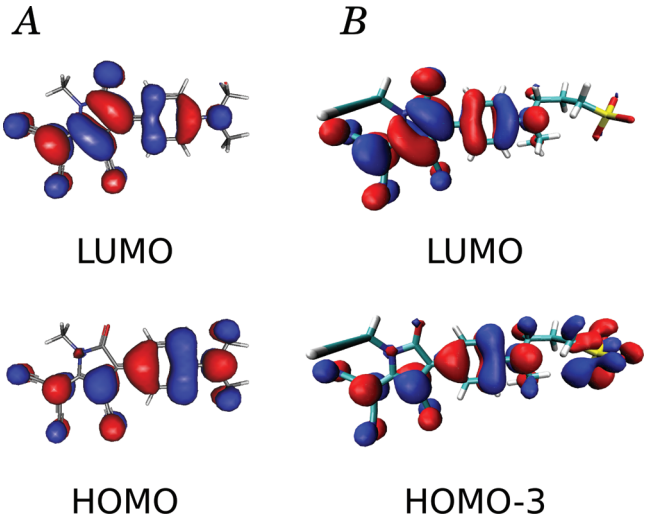


**Figure 6.** Electronic isodensity surfaces (±0.05 au) of the molecular orbitals involved in the UV−vis absorption. (A) HOMO and LUMO of the neutral model chromophore (see Scheme 4 with $R_1$ = Me, $R_2$ = Me, $R_3$ = CCH). (B) HOMO − 3 and LUMO of compound **1**.

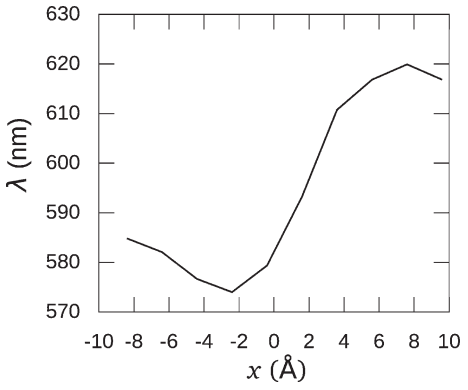


**Figure 7.** Absorption wavelength of the neutral model chromophore (Scheme 4 with $R_1$ = Me, $R_2$ = Me, $R_3$ = CCH) calculated as a function of the position of a charge ($-e$). The charge is situated at 6 Å of the $x$-axis in the $xy$ plane, and the origin is the center of the benzene ring (see Scheme 4).

BP86/ATZ2P level) of the neutral chromophore, the vertical excitation energy calculated decreases from 2.05 eV (605 nm) for a vacuum environment to 1.98 eV (626 nm) for an aqueous environment ($\varepsilon$ = 78.8).

After investigating the neutral chromophore in an equilibrium geometry, we investigated the impact of two structural parameters on the vertical excitation energies: the presence of a sulfonated tail, and mechanical deformations.

*C.2.2. Influence of a Sulfonated Tail on the Photoabsorption.* The chromophore used for the experiments contains a flexible sulfonated tail (Scheme 4 with $R_1$ = EtSO3$^-$, $R_2$ = Et, $R_3$ = CCH), which oxygen lone pairs energy lie close to the Fermi level. Depending on the position and orientation of the sulfonated group, these sulfonate orbitals may interact with $\pi$-type orbitals, leading to several frontier orbitals nearby the Fermi level participating to the photon absorption (see, for example, Figure 6B, depicting the HOMO − 3 of a typical conformation). These mixed sulfonate−$\pi$ orbitals close to the Fermi level participate in several electronic excitations in the UV−vis range. For example, for one typical conformation of the sulfonated chromophore with $\theta_2$ = 20° and $x$ = 6.6 Å, three transitions contribute to the photoabsorption at 1.90 eV ($f$ = 0.22), 2.11 eV ($f$ = 0.28), and 2.22 eV ($f$ = 0.19). These can be interpreted as a splitting of the HOMO−LUMO transition of the neutral chromophore. The presence of the sulfonate group is therefore expected to broaden the absorption band.

The impact of the charge position can be modeled by an electrostatic interaction only, using a negative point charge ($-e$) polarizing the neutral chromophore. Figure 7 illustrates the variations of the HOMO−LUMO excitation wavelength when the charge is translated along the $x$-axis. When the charge is located in the region of the HOMO ($x$ > 3 Å), the HOMO is more destabilized than the LUMO, so the excitation energy diminishes from 2.05 to 1.98 eV and the wavelength $\lambda$ increases. On the contrary, a negative charge located nearby the LUMO ($x$ < 0 Å), increases the excitation energy from 2.05 to 2.15 eV. In the MD simulations, the negative sulfonate group is on average at the position $\langle x \rangle$ = 7.50 ± 0.1 Å without the maltose and $\langle x \rangle$ = 2.15 ± 0.1 Å with the maltose. The charge may therefore shift the absorption wavelength of as much as 50 nm. Neglecting any other change, an negative charge translation toward the benzene


dx.doi.org/10.1021/jp2099015 |J. Phys. Chem. B 2012, 116, 841–851

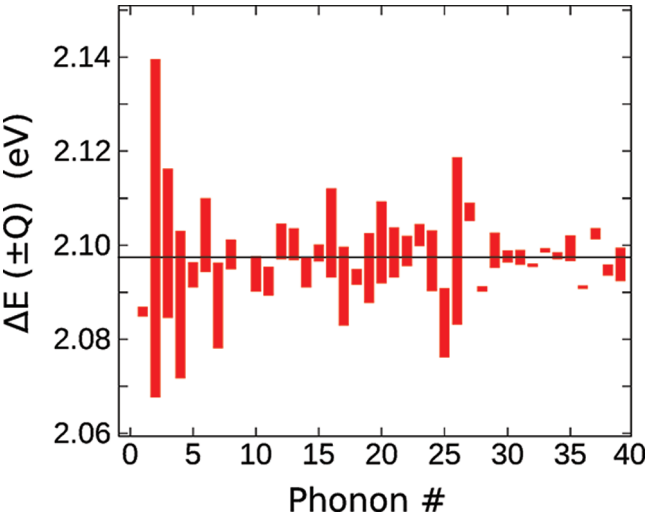


**Figure 8.** First singlet excitation energy upon deformation of the neutral model chromophore (see Scheme 4 with $R_1$ = Me, $R_2$ = Me, $R_3$ = CCH) along the first phonons with an amplitude ($|Q|$) ensuring a constant vibrational energy of 10 kJ·mol$^{-1}$. The bars join the two excitation energies obtained with the two opposite amplitudes. The phonons (B3LYP/6311+G* level) are ordered according their frequency.

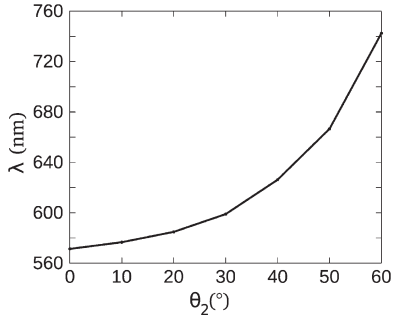


**Figure 9.** Absorption wavelength of the neutral model chromophore (see Scheme 4 with $R_1$ = Me, $R_2$ = Me, $R_3$ = CCH) calculated as a function of the dihedral angle $\theta_2$.

yields a blue shift of the vertical absorption consistent with the experimental observations.

*C.2.3. Influence of Distortion on the Neutral Nonsulfonated Chromophore.* In addition to the electrostatic embedding, the mechanical constraint exerted on the aromatic rings may also influence the absorption spectrum. The sulfonate−hydroxyl interaction is so strong that the aromatic moiety may be deformed when grafted to the sugar. The impact of various deformations on the absorption energies (i.e., the electron−phonon coupling) was estimated along each of its normal vibrational modes for the neutral chromophore (Scheme 4 with $R_1$ = Me, $R_2$ = Me, $R_3$ = CCH). Figure 8 displays the differences in energy excitations due to deformations with amplitudes $\pm|Q|$ ensuring a constant vibrational energy of 10 kJ·mol$^{-1}$. The mode numbered 2, which influences most strongly the excitation energy, corresponds almost solely to the variation of the dihedral angle $\theta_2$. An increase in $\theta_2$ favors a red shift of the absorption peak (see Figure 9). Qualitatively, this result can be understood by the different phase factors of the HOMO and LUMO on the atoms forming the dihedral angle $\theta_2$ (see Figure 6A): whereas the HOMO is bonding, therefore destabilized by torsion, the LUMO is nonbonding or antibonding, and stabilized by torsion. Concerning the influence of maltose on the gas-phase photodissociation spectrum, the MD simulations indicate that the average value of $|\theta_2|$ increases only slightly upon sugar grafting. No red shift is observed experimentally. The small modification of $|\theta_2|$ does not seem to have the leading impact on the action spectrum.

In short, several structural modifications upon sugar grafting have various effects on the optical spectra. Two relevant structural parameters with potential impact on the spectrum have been identified: the dihedral angle between the aromatic cycle, $\theta_2$, and the position of the sulfonate group. The global blue shift observed experimentally upon grafting is attributed to the apparition of cyclic conformations present in the gas phase, in which the sulfonate group is attracted toward the benzene ring by the hydroxyl groups of the maltose.

## CONCLUSIONS

In this work, carbohydrates were labeled using a push−pull chromophore based on the 4-cyano-5-dicyanomethylene-2-oxo-3-pyrroline ring, presenting a strong visible absorption. The impact of sugar grafting on the optical properties of the push−pull chromophore in the gas phase and in solution was investigated by absorption and action spectroscopy and theoretical methods.

Studies in solution and in the gas phase of the push−pull chromophore covalently bound to carbohydrates permit us to address the possible competition between intermolecular and intramolecular interactions on its optical properties. In gas-phase action spectra, the sugar moiety strongly affects the chromophore optical properties (blue shift of about −70 nm). On the contrary, the absorption spectra of the solvated chromophores are practically unchanged upon sugar grafting. These experimental approaches, combined to theoretical approaches, allowed us to better quantify the importance of intra- versus intermolecular interactions (in particular the influence of the sugar) on the structural and optical properties of the chromophore.

REMD simulations of the grafted sugars show that, in the gas phase, strong attractions between the sulfonated tail of the chromophore and the hydroxyl groups of the sugars lead to cyclic conformations, which impose mechanical constraints on the chromophore. Such cyclic conformations are much less frequent in the simulation of the solvated chromophore: water screens the electrostatic attractions and solvates both the carbohydrates and the sulfonate group. The impact of the conformation on the optical spectra was studied using TD-DFT calculations on model molecules. The observed optical shift upon grafting results from a subtle interplay between several opposite effects (polarization of the chromophore by the sulfonate group, deformation of the chromophore). We attribute the observed shift mainly to the displacement of the anionic sulfonate relative to the aromatic moiety of the chromophore. Note that we expect constraints in cyclic conformations to be weaker for long carbohydrate structures. Another interesting aspect is the fact that photodissociation within the sugar moieties is observed while the initial excitation occurs in the push−pull chromophore. This aspect and the influence of the size of the sugar on the photodissociation products, even if challenging from a theoretical point of view, need to be further explored if one has to consider visible chromophores for analytical purpose.[73]

## ASSOCIATED CONTENT

**Supporting Information.** Experimental synthesis details and characterization, absorption spectra of bare and grafted

chromophore, dissociation mass spectra of grafted glucose, and chromophore OPLS-AA parametrization. This material is available free of charge via the Internet at http://pubs.acs.org.

## AUTHOR INFORMATION

**Corresponding Author**
*E-mail: cloison@lasim.univ-lyon1.fr.

## ACKNOWLEDGMENT

The authors acknowledge the funding of the National Research Agency (ANR-09-JCJC-0077-01). Calculation time was generously provided by the Pôle Scientifique de Modélisation Numérique (ENS Lyon), by the Institut du Développement des Ressources en Information Scientifique (IDRIS), and by the Centre Informatique national de l'Enseignement Supérieur (CINES), project x2011085142. Amandine Racaud thanks SANOFI-AVENTIS for generous support.

## REFERENCES

(1) Jelinek, R.; Kolusheva, S. *Chem. Rev.* **2004**, *104*, 5987.
(2) Harwood, G. W.; Pouton, C. W. *Adv. Drug Delivery Rev.* **1996**, *18*, 163.
(3) Wilson, G. S.; Gifford, R. *Biosens. Bioelectron.* **2005**, *20*, 2388.
(4) Karyakin, A. A.; Gitelmacher, O. V.; Karyakina, E. E. *Anal. Chem.* **1995**, *67*, 2419.
(5) Krysteva, M. A.; Yotova, L. K. *J. Chem. Technol. Biotechnol.* **1992**, *54*, 13.
(6) Cao, H. S.; Heagy, M. D. *J. Fluoresc.* **2004**, *14*, 569.
(7) James, T. D.; Shinkai, S. Artificial receptors as chemosensors for carbohydrates. In *Host−Guest Chemistry*; Penadés, S., Ed.; Springer-Verlag: Berlin, Germany, 2002; Vol. 218; p 159.
(8) Anumula, K. R. *Anal. Biochem.* **2006**, *350*, 1.
(9) Starr, C. M.; Masada, R. I.; Hague, C.; Skop, E.; Klock, J. C. *J. Chromatogr., A* **1996**, *720*, 295.
(10) Lamari, F. N.; Kuhn, R.; Karamanos, N. K. *J. Chromatogr., B* **2003**, *793*, 15.
(11) Ko, B. J.; Brodbelt, J. S. *J. Mass Spectrom.* **2011**, *46*, 359.
(12) Wilson, J. J.; Brodbelt, J. S. *Anal. Chem.* **2008**, *80*, 5186.
(13) Matsumoto, H.; Imai, H. T. S. Ger. Offen. 3716840 A1, 1987.
(14) Carboni, R. A. U.S. Patent 3013013, 1961.
(15) Jang, S.-H.; Luo, J.; Tucker, N. M.; Leclercq, A.; Zojer, E.; Haller, M. A.; Kim, T.-D.; Kang, J.-W.; Firestone, K.; Bale, D.; Lao, D.; Benedict, J. B.; Cohen, D.; Kaminsky, W.; Kahr, B.; Bredas, J.-L.; Reid, P.; Dalton, L. R.; Jen, A. K. Y. *Chem. Mater.* **2006**, *18*, 2982.
(16) Fadda, E.; Woods, R. *Drug Discovery Today* **2010**, 596.
(17) Shen, T.; Langan, P.; French, A.; Johnson, G.; Gnanakaran, S. *J. Am. Chem. Soc.* **2009**, *131*, 14786.
(18) Damm, W.; Frontera, A.; Tirado-Rives, J.; Jorgensen, W. *J. Comput. Chem.* **1997**, *18*, 1955.
(19) Guvench, O.; Hatcher, E.; Venable, R.; Pastor, R.; Mackerell, A. *J. Chem. Theory Comput.* **2009**, *5*, 2353.
(20) Hansen, H.; Hanenberger, P. *J. Comput. Chem.* **2011**, *32*, 998.
(21) Kirschner, K.; Yongye, A.; Tschampel, S.; Gonzalez-Outeirio, J.; Daniels, C.; Foley, L.; Woods, R. *J. Comput. Chem.* **2008**, *29*, 622.
(22) Kony, D.; Damm, W.; Stoll, S.; Van Gunsteren, W. F. *J. Comput. Chem.* **2002**, *23*, 1416.
(23) Lins, R.; Hanenberger, P. *J. Comput. Chem.* **2005**, *26*, 1400.
(24) Raman, P.; Guvench, O.; MacKerell, A. *J. Phys. Chem. B* **2010**, *114*, 12981.
(25) Senderowitz, H.; Still, C. *J. Org. Chem.* **1997**, *62*, 1427.
(26) Stortz, C.; Johnson, G.; French, A.; Csonka, G. B. *Carbohydr. Res.* **2009**, *344*, 2217.
(27) Lopez, C.; Rzepiela, A.; de Vries, A.; Dijkhuizen, L.; Hunenberger, P.; Marrink, S. *J. Chem. Theory Comput.* **2009**, *5*, 3195.
(28) Shen, T.; Langan, P.; French, A.; Johnson, G.; Gnanakaran, S. *J. Am. Chem. Soc.* **2009**, *131*, 14786.
(29) Jacquemin, D.; Perpète, E.; Ciofini, I.; Adamo, A. *Acc. Chem. Res.* **2009**, *42*, 326.
(30) Runge, E.; Gross, E. K. U. *Phys. Rev. Lett.* **1984**, *52*, 997.
(31) Loison, C.; Antoine, R.; Broyer, M.; Dugourd, P.; Guthmuller, J.; Simon, D. *Chem.—Eur. J.* **2008**, *14*, 7351.
(32) Garavelli, M. *Theor. Chem. Acc.* **2006**, *116*, 87.
(33) Werner, H. J.; Knowles, P. J. *J. Chem. Phys.* **1985**, *82*, 5053.
(34) Loison, C.; Simon, D. *J. Phys. Chem. A* **2010**, *114*, 7769.
(35) Senn, H. M.; Thiel, W. *Angew. Chem., Int. Ed.* **2009**, *48*, 1198.
(36) Melaccio, F.; Olivucci, M.; Lindh, R.; Ferré, N. *Int. J. Quantum Chem.* **2011**, *111*, 3339.
(37) Mittelbach, M. *Monatsh. Chem.* **1985**, *116*, 689.
(38) Tanaka, T.; Nagai, H.; Noguchi, M.; Kobayashi, A.; Shoda, S.-I. *Chem. Commun.* **2009**, 3378.
(39) For an example of microwave-assisted copper(I)-catalysed azide−alkyne cycloadditions, see: Cecioni, S.; Lalor, R.; Blanchard, B.; Praly, J.-P.; Imberty, A.; Matthews, S. E.; Vidal, S. *Chem.—Eur. J.* **2009**, *15*, 13232–13240.
(40) Larraillet, V.; Antoine, R.; Dugourd, P.; Lemoine, J. *Anal. Chem.* **2009**, *81*, 8410.
(41) Racaud, A.; Antoine, R.; Joly, L.; Mesplet, N.; Dugourd, P.; Lemoine, J. *J. Am. Soc. Mass Spectrom.* **2009**, *20*, 1645.
(42) te Velde, G.; Bickelhaupt, F. M.; Baerends, E. J.; Fonseca Guerra, C.; van Gisbergen, S. J. A.; Snijders, J. G.; Ziegler, T. *J. Comput. Chem.* **2001**, *22*, 931.
(43) Frisch, M. J.; Trucks, G. W.; Schlegel, H. B.; Scuseria, G. E.; Robb, M. A.; Cheeseman, J. R.; Scalmani, G.; Barone, V.; Mennucci, B.; Petersson, G. A.; Nakatsuji, H.; Caricato, M.; Li, X.; Hratchian, H. P.; Izmaylov, A. F.; Bloino, J.; Zheng, G.; Sonnenberg, J. L.; Hada, M.; Ehara, M.; Toyota, K.; Fukuda, R.; Hasegawa, J.; Ishida, M.; Nakajima, T.; Honda, Y.; Kitao, O.; Nakai, H.; Vreven, T.; Montgomery, J. A., Jr.; Peralta, J. E.; Ogliaro, F.; Bearpark, M.; Heyd, J. J.; Brothers, E.; Kudin, K. N.; Staroverov, V. N.; Kobayashi, R.; Normand, J.; Raghavachari, K.; Rendell, A.; Burant, J. C.; Iyengar, S. S.; Tomasi, J.; Cossi, M.; Rega, N.; Millam, J. M.; Klene, M.; Knox, J. E.; Cross, J. B.; Bakken, V.; Adamo, C.; Jaramillo, J.; Gomperts, R.; Stratmann, R. E.; Yazyev, O.; Austin, A. J.; Cammi, R.; Pomelli, C.; Ochterski, J. W.; Martin, R. L.; Morokuma, K.; Zakrzewski, V. G.; Voth, G. A.; Salvador, P.; Dannenberg, J. J.; Dapprich, S.; Daniels, A. D.; Farkas, Ö.; Foresman, J. B.; Ortiz, J. V.; Cioslowski, J.; Fox, D. J. *Gaussian 09*, revision A.02; Gaussian, Inc.: Wallingford, CT, 2009.
(44) Becke, A. D. *Phys. Rev. A* **1988**, *38*, 3098.
(45) Perdew, J. *Phys. Rev. B* **1986**, *33*, 8822.
(46) Zhao, Y.; Truhlar, D. *Acc. Chem. Res.* **2008**, *41*, 157.
(47) van Gisbergen, S. J. A.; Guerra, F.; Baerends, E. J. *J. Comput. Chem.* **2000**, *21*, 1511.
(48) Zangwill, A.; Soven, P. *Phys. Rev. Lett.* **1980**, *45*, 204.
(49) Schipper, P. R. T.; Gritsenko, O. V.; van Gisbergen, S. J. A.; Baerends, E. J. *J. Chem. Phys.* **2000**, *112*, 1344.
(50) Tomasi, J.; Mennucci, B.; Cammi, R. *Chem. Rev.* **2005**, *105*, 2999.
(51) Allouche, A.-R. *J. Comput. Chem.* **2011**, *32*, 174.
(52) McDonald, N.; Jorgensen, W. *J. Phys. Chem. B* **1998**, *102*, 8049.
(53) Bayly, C.; Cieplak, P.; Cornell, W.; Kollman, P. *J. Phys. Chem.* **1993**, *97*, 10269.
(54) Dupradeau, F.-Y.; Pigache, A.; Zaffran, T.; Savineau, C.; Lelong, R.; Grivel, N.; Lelong, D.; Rosanski, W.; Cieplak, P. *Phys. Chem. Chem. Phys.* **2010**, *12*, 7821.
(55) Wang, J.; Cieplak, P.; Kollman, P. *J. Comput. Chem.* **2000**, *21*, 1049.
(56) Jorgensen, W.; Tirado-Rives, J. *J. Comput. Chem.* **2005**, *26*, 1689.
(57) Vaiana, A.; Cournia, Z.; Costescu, I.; Smith, J. *Comput. Phys. Commun.* **2005**, *167*, 34.
(58) Nelder, J. A.; Mead, R. *Comput. J.* **1965**, *7*, 308.
(59) Patriksson, A.; Spoel, D. *Phys. Chem. Chem. Phys.* **2008**, *10*, 2073.
(60) Sugita, Y.; Kitao, A.; Okamoto, Y. *J. Chem. Phys.* **2000**, *113*, 6042.

(61) Hess, B.; Kutzner, C.; van der Spoel, D.; Lindahl, E. *J. Chem. Theory Comput.* **2008**, *4*, 435.
(62) Bussi, G.; Donadio, D.; Parrinello, M. *J. Chem. Phys.* **2007**, *126*, 014101.
(63) Rosta, E.; Buchete, N.-V.; Hummer, G. *J. Chem. Theory Comput.* **2009**, *5*, 1393.
(64) Sindhikara, D.; Meng, Y.; Roitberg, A. *J. Chem. Phys.* **2008**, *128*, 024103.
(65) Humphrey, W. *J. Mol. Graphics* **1996**, *14*, 33.
(66) Jorgensen, W. L.; Chandrasekhar, J.; Madura, J. D.; Impey, R. W.; Klein, M. L. *J. Chem. Phys.* **1983**, *79*, 926.
(67) Reichardt, C. *Chem. Rev.* **1994**, *94*, 2319.
(68) Devakumar, A.; Mechref, Y.; Kang, P.; Novotny, M. V.; Reilly, J. P. *Rapid Commun. Mass Spectrom.* **2007**, *21*, 1452.
(69) Devakumar, A.; Mechref, Y.; Kang, P.; Novotny, M. V.; Reilly, J. P. *J. Am. Soc. Mass Spectrom.* **2008**, *19*, 1027.
(70) Devakumar, A.; Thompson, M. S.; Reilly, J. P. *Rapid Commun. Mass Spectrom.* **2005**, *19*, 2313.
(71) Racaud, A.; Allouche, A. R.; Antoine, R.; Lemoine, J.; Dugourd, P. *J. Mol. Struct.: THEOCHEM* **2010**, *960*, 51.
(72) Reilly, J. P. *Mass Spectrom. Rev.* **2009**, *28*, 425.
(73) Enjalbert, Q.; Simon, R.; Salvador, A.; Antoine, R.; Redon, S.; Ayhan, M. M.; Darbour, F.; Chambert, S.; Bretonnière, Y.; Dugourd, P.; Lemoine, J. *Rapid Commun. Mass Spectrom.* **2011**, *25*, 3375.